

# A fast spinning magnetic white dwarf in the double-degenerate, super-Chandrasekhar system NLTT 12758 <sup>★</sup>

Adela Kawka<sup>1†</sup>, Gordon P. Briggs<sup>2</sup>, Stéphane Vennes<sup>1,3</sup>, Lilia Ferrario<sup>2</sup>  
Ernst Paunzen<sup>4</sup> and Dayal T. Wickramasinghe<sup>2</sup>

<sup>1</sup>*Astronomický ústav AV ČR, Fričova 298, 251 65 Ondřejov, Czech Republic*

<sup>2</sup>*Mathematical Sciences Institute, The Australian National University, Canberra, ACT 0200, Australia*

<sup>3</sup>*Visitor at Mathematical Sciences Institute, The Australian National University, Canberra, ACT 0200, Australia*

<sup>4</sup>*Department of Theoretical Physics and Astrophysics, Masaryk University, Kotlářská 2, 611 37 Brno, Czech Republic*

Accepted XXX. Received YYY; in original form ZZZ

## ABSTRACT

We present an analysis of the close double degenerate NLTT 12758, which is comprised of a magnetic white dwarf with a field of about 3.1 MG and an apparently non-magnetic white dwarf. We measured an orbital period of 1.154 days and found that the magnetic white dwarf is spinning around its axis with a period of 23 minutes. An analysis of the atmospheric parameters has revealed that the cooling ages of the two white dwarfs are comparable, suggesting that they formed within a short period of time from each other. Our modelling indicates that the non-magnetic white dwarf is more massive ( $M = 0.83 M_{\odot}$ ) than its magnetic companion ( $M = 0.69 M_{\odot}$ ) and that the total mass of the system is higher than the Chandrasekhar mass. Although the stars will not come into contact over a Hubble time, when they do come into contact, dynamically unstable mass transfer will take place leading to either an accretion induced collapse into a rapidly spinning neutron star or a Type Ia supernova.

**Key words:** stars: magnetic fields – stars: individual: NLTT 12758 – white dwarfs – binaries: close

## 1 INTRODUCTION

The majority of stars will evolve into a white dwarf and a significant fraction of white dwarfs harbours a magnetic field that ranges from a few kG to about 1000 MG (Liebert et al. 2003; Kawka et al. 2007). Spectroscopic and spectropolarimetric surveys (e.g., Schmidt & Smith 1995; Schmidt et al. 2001; Aznar Cuadrado et al. 2004; Kawka et al. 2007; Kawka & Vennes 2012a; Landstreet et al. 2012; Kepler et al. 2013) of white dwarfs have been able to place constraints on the incidence of magnetism among white dwarfs. The incidence of magnetic white dwarfs in the local neighbourhood has been estimated by Kawka et al. (2007) to be around 20 %. The local sample, as well as various surveys, have shown that the incidence of magnetism as a function of field strength is constant, although Landstreet et al. (2012) suggested a possible field resurgence at the extremely low-field ( $< 1$  kG) end of the distribution. A higher incidence of magnetism is also observed in cool polluted white dwarfs. Kawka & Vennes (2014) found an

incidence of  $\approx 40$  % in cool ( $T_{\text{eff}} < 6000$  K) DAZ<sup>1</sup> white dwarfs. A higher incidence of magnetism was also observed among cool DZ<sup>2</sup> white dwarfs (Hollands et al. 2015). A recent review on the properties of magnetic white dwarfs can be found in Ferrario et al. (2015a).

The origin of large scale magnetic fields in stars is still one of the main unanswered questions in astrophysics, although recent data, particularly from surveys such as the Sloan Digital Sky Survey (SDSS, York et al. 2000), the Magnetism in Massive Stars (MiMeS, Wade et al. 2016) and the Binarity and Magnetic Interactions in various classes of stars (BinaMiCS, Alecian et al. 2015) may have finally thrown some light into this matter (Ferrario et al. 2015b). Magnetism in white dwarfs has been explained with two main evolutionary scenarios. For a long time the leading theory was that the progenitors of magnetic white dwarfs are magnetic Ap and Bp stars (Angel et al. 1981). Under the assumption of magnetic flux conservation, the magnetic field strengths observed in Ap stars would correspond to magnetic fields in white dwarfs in excess of 10 MG (Kawka & Vennes 2004; Tout et al.

<sup>★</sup> Based on observations made with ESO telescopes at the La Silla Paranal Observatory under programmes 083.D-0540, 084.D-0862, 089.D-0864 and 090.D-0473. Based in part on data collected with the Danish 1.54-m telescope at the ESO La Silla Observatory.

<sup>†</sup> E-mail: kawka@asu.cas.cz

<sup>1</sup> DAZ type white dwarfs show photospheric hydrogen (DA) and metal lines.

<sup>2</sup> DZ type white dwarfs show metal lines only.

2004; Wickramasinghe & Ferrario 2005). The progenitors of white dwarfs with weaker fields may be other main-sequence stars whose magnetic fields are below our current detection limits or could be dynamo-generated in later stages of stellar evolution.

More recently, proposals that strong magnetic fields are created in evolving interacting binaries via a dynamo mechanism during a common envelope (CE) phase (Tout et al. 2008; Potter & Tout 2010; Nordhaus et al. 2011; García-Berro et al. 2012; Wickramasinghe et al. 2014) have gained momentum as a possible origin for strong magnetic fields in white dwarfs. The main reason for this proposal is that all magnetic white dwarfs appear to be either single or in interacting binaries (the magnetic cataclysmic variables). That is, magnetic white dwarfs are never found paired with a non-interacting, non-degenerate star, which is at odds with the fact that approximately 30% of all non-magnetic white dwarfs are found in non-interacting binaries with a non-degenerate companion (usually an M-dwarf) (Liebert et al. 2005; Ferrario 2012; Liebert et al. 2015). This result is hard to explain and leaves the magnetic cataclysmic variables without obvious progenitors. Because of this observational peculiarity, the existence of magnetic fields in white dwarfs has been linked to fields generated during CE binary interactions or mergers. The merger scenario during the CE also successfully explains the higher than average mass of isolated magnetic white dwarfs (Briggs et al. 2015). The complex magnetic field structure usually observed in rotating high field magnetic white dwarfs would also be in support of a merging hypothesis.

However, a few common-proper motion (CPM) magnetic plus non-magnetic double degenerate systems are now known (Ferrario et al. 1997; Girven et al. 2010; Dobbie et al. 2012, 2013). In some of these cases, the more massive magnetic white dwarf is hotter and hence younger than its non-magnetic companion, which seems to imply that the more massive star evolved later. This apparent paradox can be resolved by postulating that systems of this kind were initially triple systems and that the magnetic white dwarf resulted from the merger of two of the three stars (e.g., EUVE J0317–855, Ferrario et al. 1997).

The study of the magnetic field structure in white dwarfs may also give us important clues on how they formed. Normally, a simple dipole is assumed for the field structure, but the study of rotating magnetic white dwarfs have all shown variability, hence revealing much more complex structures. One of the most extreme examples of a rotating magnetic white dwarf is the hot ( $T \approx 34\,000$  K) and massive ( $M \approx 1.35 M_{\odot}$ ) EUVE J0317–855, which has a rotation period of 12 minutes (Barstow et al. 1995; Ferrario et al. 1997). The rotation of the white dwarf reveals a two component magnetic field structure: A high field magnetic spot ( $B \geq 425$  MG) with an underlying lower field (Vennes et al. 2003). Another example of a rotating white dwarf with a complex magnetic field structure is WD 1953–011 (Maxted et al. 2000; Valyavin et al. 2008). In this case, the rotation is slower ( $P_{\text{rot}} = 1.448$  days Brinkworth et al. 2005) and the magnetic field strength is much weaker (180 kG – 520 kG) than that of EUVE J0317–855.

NLTT 12758 was discovered to be a magnetic white dwarf by Kawka & Vennes (2012a). They showed that the circular polarization spectra are variable and that there is also variability in the H $\alpha$  core suggesting that NLTT 12758 is a close double degenerate system. Here, we present our analysis of spectroscopic, spectropolarimetric and photometric data of NLTT 12758. The observations are presented in Section 2. The orbital and rotation period analyses are described in Sections 3.1 and 3.2, respectively. The stellar and atmospheric parameters are presented in Section 3.3, and we discuss

the evolutionary scenarios in Section 3.4. We discuss the case of NLTT 12758 in comparison to other known double degenerate systems containing a magnetic white dwarf in Section 4 and we conclude in Section 5.

## 2 OBSERVATIONS

### 2.1 Spectroscopy and Spectropolarimetry

NLTT 12758 was first observed with the R.-C. spectrograph attached to the 4m telescope at Cerro Tololo Inter-American Observatory (CTIO) on UT 2008 February 24. We used the KPGL2 (316 lines per mm) grating with the slit-width set to 1.5 arcsec providing a resolution of about 8 Å. We obtained a second set of low-dispersion spectra with the EFOSC2 spectrograph attached to the New Technology Telescope (NTT) at La Silla. Two consecutive spectra were obtained on UT 2009 08 27. We used grism number 11 and set the slit-width to 1.0 arcsec providing a resolution of about 14 Å. Both sets of spectra revealed Zeeman splitting in the Balmer lines. Figure 1 shows the low dispersion spectra.

We obtained a first set of spectropolarimetric observations using the FOCal Reducer and low dispersion Spectrograph (FORSD2) attached to the 8m telescope (UT1) of the European Southern Observatory (ESO) in 2009. We obtained another set of observations using the same set-up in 2013. We used the 1200 lines mm<sup>-1</sup> grism (1200R+93) centred on H $\alpha$  providing a spectral dispersion of 0.73 Å pixel<sup>-1</sup>. We set the slit-width to 1 arcsec providing a spectral resolution of 3.0 Å. Each spectropolarimetric observation consisted of two individual exposures, with the first having the Wollaston prism rotated to  $-45^\circ$  immediately followed by the second exposure with the Wollaston prism rotated to  $+45^\circ$ .

We also obtained five spectra of NLTT 12758 with the EFOSC2 spectrograph in September 2012. These spectra were obtained with grism number 20 which provides a spectral dispersion of 1.09 Å per binned pixel. The slit-width was set to 0.7 arcsec providing a resolution of 3.0 Å.

Finally we obtained a set of five consecutive spectra of NLTT 12758 with the X-shooter spectrograph (Vernet et al. 2011) attached to the VLT at Paranal Observatory on UT 2014 August 26. The spectra were obtained with the slit width set to 0.5, 0.9 and 0.6 arcsec for the UVB, VIS and NIR arms, respectively. This setup provided a resolution of  $R = 9000, 7450$  and  $7780$  for the UVB, VIS and NIR arms, respectively.

The log of the spectroscopic observations is presented in Table 1.

### 2.2 Photometry

We collected available photometric measurements from the Galaxy Evolutionary Explorer (GALEX) sky survey, optical photometry from Eggen (1968) and the AAVSO Photometric All-Sky Survey, Deep Near Infrared Survey (DENIS) of the southern sky, the Two Micron All Sky Survey (2MASS) and the Wide-field Infrared Survey Explorer (WISE). These measurements are listed in Table 2.

We obtained new CCD photometric measurements with the 1.54-m Danish telescope at the La Silla Observatory in Chile on UT 26th December 2014, 30th January 2015 and 11th March 2016. On 26th December 2014, we alternated between the V and R filter and on 30th January 2015 11th March 2016 we observed NLTT 12758 with the R filter only. The integration time was set to 40 seconds

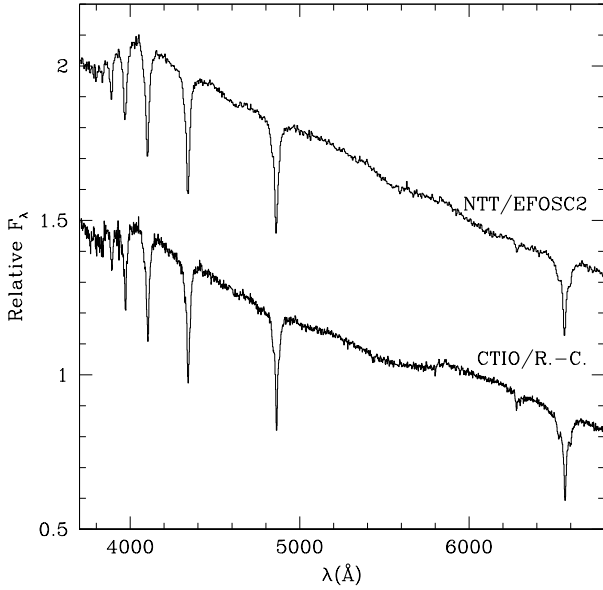


**Figure 1.** Low dispersion CTIO/R.-C. and NTT/EFOSC2 spectra of NLTT 12758 revealing Zeeman splitted Balmer lines.

for all observations. The data reduction and differential photometry were performed using the C-Munipack package<sup>3</sup>. Since several comparison stars were available, and these were checked individually to exclude variable objects. We compared the results of the final differential light curves using the aperture photometry routine from IRAF (Stetson 1987). We found no differences above the photon noise.

### 3 ANALYSIS

During the first spectropolarimetric observations of NLTT 12758, we found that the  $\sigma$  components of H $\alpha$  varied with a reversal in the polarisation spectra, thus revealing itself as a new member of the DAP white dwarf class<sup>4</sup>. We also found that the width of the core of the  $\pi$  component is structured and variable, thus suggesting the presence of a close companion. The FORS2, EFOSC2 and X-shooter spectra displayed in Figure 2 clearly show the variations in the central H $\alpha$  core. The resolution of the X-shooter spectra and timing of the observations allowed us to discern the individual cores of the two components.

#### 3.1 Binary parameters

We measured the radial velocity of the magnetic white dwarf by first subtracting a template representing the DA white dwarf and then cross-correlating the DAP white dwarf FORS/EFOSC2 spectra ( $\sigma$  components only) with the X-shooter spectrum. The DA radial velocity could only be measured at quadrature, i.e. at maximum line core separation, and with a sufficient signal-to-noise ratio. Only

<sup>3</sup> <http://c-munipack.sourceforge.net/>

<sup>4</sup> DAP white dwarfs show hydrogen lines with detectable polarisation. The DAH classification is reserved for Zeeman splitted line spectra, but without confirmed polarization.

**Table 1.** Spectroscopic observation log

UT date	UT start	Exposure time (s)	Instrument/Telescope
24 Feb 2008	02:04:42	1200	RC/CTI04m
24 Feb 2008	02:26:56	1200	RC/CTI04m
27 Aug 2009	09:39:21	600	EFOSC2/NTT
27 Aug 2009	09:49:57	600	EFOSC2/NTT
23 Oct 2009	06:35:09	900	FORS2/UT1
23 Oct 2009	06:51:18	900	FORS2/UT1
23 Oct 2009	07:16:20	900	FORS2/UT1
23 Oct 2009	07:32:28	900	FORS2/UT1
23 Oct 2009	07:55:18	900	FORS2/UT1
23 Oct 2009	08:11:35	900	FORS2/UT1
24 Nov 2009	02:40:00	900	FORS2/UT1
24 Nov 2009	02:56:08	900	FORS2/UT1
24 Nov 2009	03:24:14	900	FORS2/UT1
24 Nov 2009	03:40:22	900	FORS2/UT1
02 Sep 2012	08:41:00	900	EFOSC2/NTT
02 Sep 2012	09:04:14	900	EFOSC2/NTT
03 Sep 2012	08:09:10	900	EFOSC2/NTT
03 Sep 2012	08:33:13	900	EFOSC2/NTT
03 Sep 2012	09:18:43	900	EFOSC2/NTT
04 Jan 2013	03:49:14	700	FORS2/UT1
04 Jan 2013	04:02:02	700	FORS2/UT1
04 Jan 2013	04:15:06	700	FORS2/UT1
04 Jan 2013	04:27:55	700	FORS2/UT1
04 Jan 2013	04:41:01	700	FORS2/UT1
04 Jan 2013	04:53:49	700	FORS2/UT1
07 Jan 2013	02:39:34	700	FORS2/UT1
07 Jan 2013	02:52:22	700	FORS2/UT1
07 Jan 2013	03:05:26	700	FORS2/UT1
07 Jan 2013	03:18:14	700	FORS2/UT1
07 Jan 2013	03:31:18	700	FORS2/UT1
07 Jan 2013	03:44:06	700	FORS2/UT1
07 Jan 2013	03:57:28	700	FORS2/UT1
07 Jan 2013	04:10:17	700	FORS2/UT1
07 Jan 2013	04:33:02	700	FORS2/UT1
07 Jan 2013	04:46:02	700	FORS2/UT1
03 Feb 2013	03:01:49	700	FORS2/UT1
03 Feb 2013	03:14:38	700	FORS2/UT1
03 Feb 2013	03:27:35	700	FORS2/UT1
03 Feb 2013	03:40:24	700	FORS2/UT1
03 Feb 2013	03:53:22	700	FORS2/UT1
03 Feb 2013	04:06:10	700	FORS2/UT1
26 Aug 2014	08:18:30	450/540 <sup>1</sup>	Xshooter/UT3
26 Aug 2014	08:28:43	450/540 <sup>1</sup>	Xshooter/UT3
26 Aug 2014	08:37:51	450/540 <sup>1</sup>	Xshooter/UT3
26 Aug 2014	08:47:00	450/540 <sup>1</sup>	Xshooter/UT3
26 Aug 2014	08:56:08	450/540 <sup>1</sup>	Xshooter/UT3

<sup>1</sup> Exposure times for the VIS/UVB arms, respectively.

three sets of spectra met these criteria. Consecutive exposures (2 to 4) were co-added to increase the signal-to-noise and improve the reliability of the velocity measurements while minimizing orbital smearing. Table 3 lists the barycentric julian date (BJD) with the measured radial velocities of the magnetic and non-magnetic white dwarfs in NLTT 12758. All velocities are barycentric corrected.

We searched for a period in the measurements using  $\chi^2$  minimization techniques by fitting the sinusoidal function  $v = \gamma + K \times \sin(2\pi(t - T_0)/P)$  to the measured radial velocities where  $t$  is time (BJD). The initial epoch ( $T_0$ ), period ( $P$ ), mean velocity ( $\gamma$ ) and velocity semi-amplitude ( $K$ ) were determined simultaneously and we normalized the  $\chi^2$  function by setting the minimum reduced  $\chi^2$  to 1.

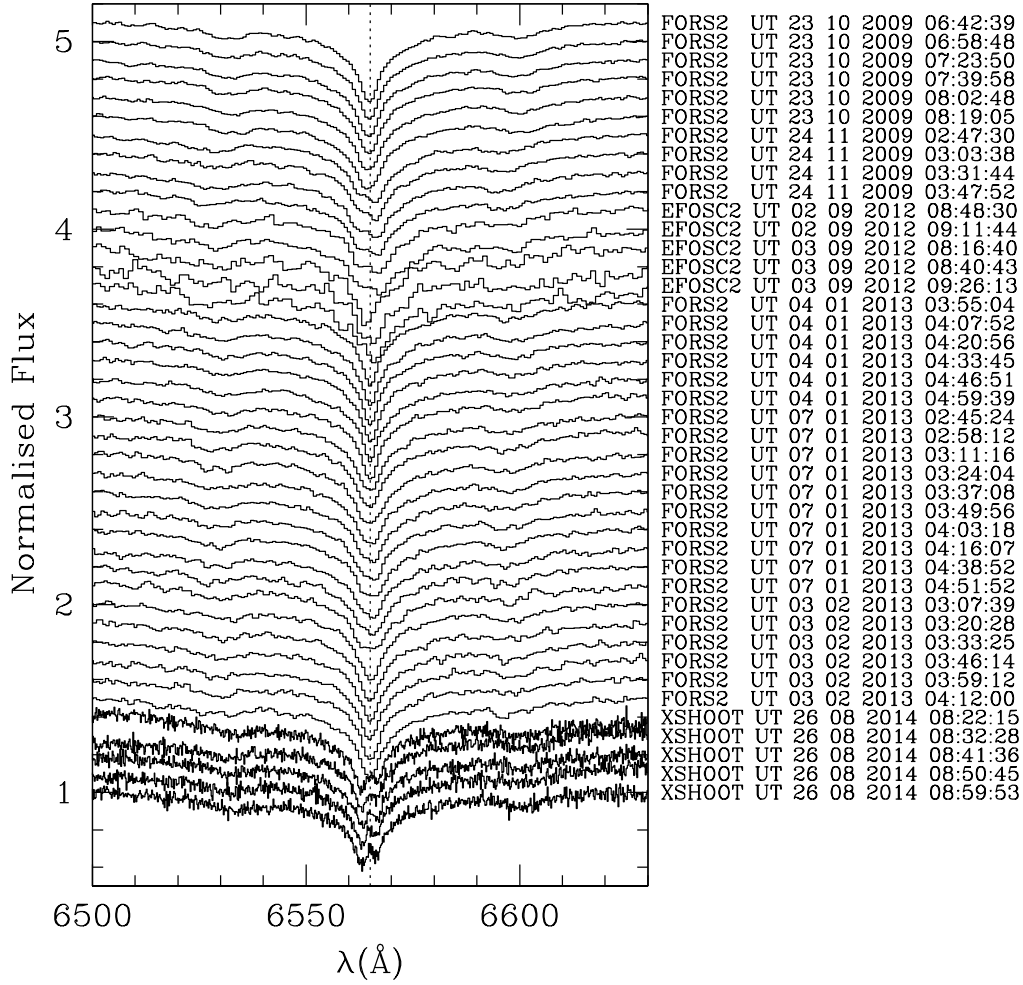


**Figure 2.** EFOSC2, FORS2 and X-shooter spectra of NLTT 12758 showing variations in the H $\alpha$  core. The mid-exposure UT time is listed for each spectrum.

**Table 2.** Photometric measurements of NLTT 12758

Band	Magnitude	Reference
<i>GALEX FUV</i>	not detected	1
<i>GALEX NUV</i>	$17.401 \pm 0.016$	1
<i>V</i>	$15.46, 15.483 \pm 0.071$	2,3
<i>B - V</i>	+0.31	2
<i>U - B</i>	-0.71	2
<i>B</i>	$15.855 \pm 0.094$	3
<i>g</i>	$15.607 \pm 0.037$	3
<i>r</i>	$15.417 \pm 0.074$	3
<i>i</i>	$15.443 \pm 0.132$	3
DENIS <i>I</i>	$14.976 \pm 0.07$	4
DENIS <i>J</i>	$14.713 \pm 0.15$	4
2MASS <i>J</i>	$14.809 \pm 0.032$	5
2MASS <i>H</i>	$14.723 \pm 0.071$	5
2MASS <i>K</i>	$14.683 \pm 0.096$	5
WISE W1	$14.703 \pm 0.034$	6
WISE W2	$14.781 \pm 0.069$	6

References: (1) [Morrissey et al. \(2007\)](#); (2) [Eggen \(1968\)](#); (3) [Henden et al. \(2016\)](#); (4) [Fouqué et al. \(2000\)](#); (5) [Skrutskie et al. \(2006\)](#); (6) [Cutri et al. \(2012\)](#)

**Table 3.** Radial velocity measurements

BJD (2450000+)	$v_{DAP}$ (km s $^{-1}$ )	$v_{DA}$ (km s $^{-1}$ )
5127.78952	$157 \pm 6$	...
5127.81811	$165 \pm 5$	...
5127.84523	$196 \pm 5$	...
5159.62676	$2 \pm 8$	...
5159.64212	...	$156 \pm 20$
5159.65748	$18 \pm 8$	...
6172.87606	$18 \pm 7$	$196 \pm 20$
6173.86764	$35 \pm 8$	...
6296.67107	$112 \pm 6$	...
6296.68904	$120 \pm 7$	...
6296.70703	$124 \pm 6$	...
6299.62701	$47 \pm 7$	...
6299.65848	$38 \pm 8$	...
6299.69457	$29 \pm 9$	...
6326.64042	$100 \pm 6$	...
6326.66725	$79 \pm 6$	...
6895.86223	$193 \pm 5$	$12 \pm 5$



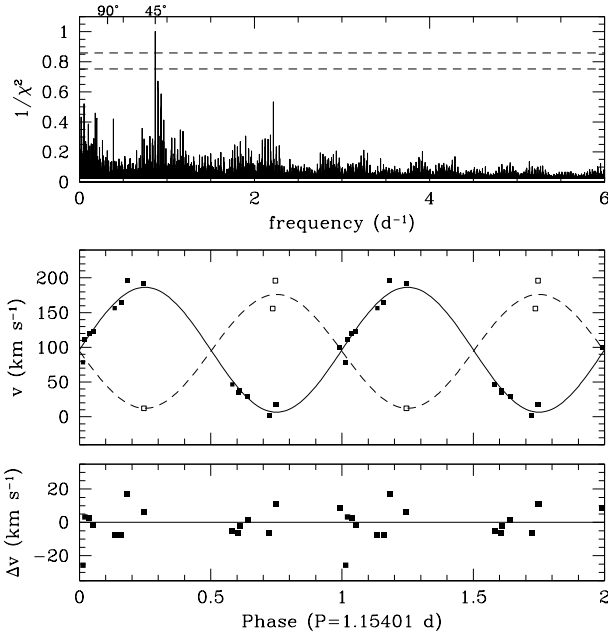


**Figure 3.** (Top panel) period analysis of the FORS2, EFOC2 and X-shooter data with 66 and 90% confidence level (dashed lines). (Middle panel) radial velocity measurements (Table 3) of the DA (open squares) and DAP stars (full squares) phased on the orbital period and the best-fitting sine curves (Table 4) and (bottom panel) velocity residuals for the DAP star. The longest period is marked at  $90^\circ$  on the top horizontal axis along with the actual period at  $45^\circ$ .

Figure 3 shows the period analysis of the FORS2, EFOC2 and X-shooter data sets and Table 4 lists the new binary parameters. Using the FORS2 and EFOC2 data combined with the X-shooter data we determined a period of  $1.15401 \pm 0.00005$  days and a velocity semi-amplitude for the DAP star of  $89.7 \pm 3.8 \text{ km s}^{-1}$  with an average residual of only  $7.7 \text{ km s}^{-1}$  and commensurate with measurement errors (Table 3). The corresponding mass function is  $f(M_{\text{DA}}) = 0.0863 \pm 0.0110 M_\odot$ . Since the X-shooter spectra were taken near quadrature and clearly show the cores of both components, we were able to estimate a semi-amplitude of  $81.9 \pm 17.3 \text{ km s}^{-1}$  for the non-magnetic white dwarf. The orbital mass ratio  $M_{\text{DA}}/M_{\text{DAP}} = 0.85 - 1.35$  is not sufficiently accurate to constrain the evolution of the system, and additional constraints will be provided by the spectroscopic analysis (Section 3.3.2).

### 3.2 Rotation

The spectropolarimetric data have revealed a modulation that we attribute to the rotation of the magnetic white dwarf.

We measured the integrated polarization for both  $\sigma$  components and conducted a period search. Two significant periods at 22.6 minutes and 9 minutes stand out. Since some of the exposure times were longer than 9 minutes, it is unlikely that the 9 minutes period is real. Figure 4 shows line polarization measurements obtained by integrating  $V/I$  over the wavelength range ( $\approx \pm 20 \text{ \AA}$ ) covered by the individual  $\sigma$  components phased on the 22.6 minute period. Both  $\sigma$  components show sinusoidal behaviour and a symmetry about the null polarization axis which imply that the magnetic poles spend nearly equal time in the field-of-view.

Figure 5 shows the co-added FORS2 circular polarization spectra over three separate ranges of a rotation cycle ( $P = 22.6 \text{ min}$ )

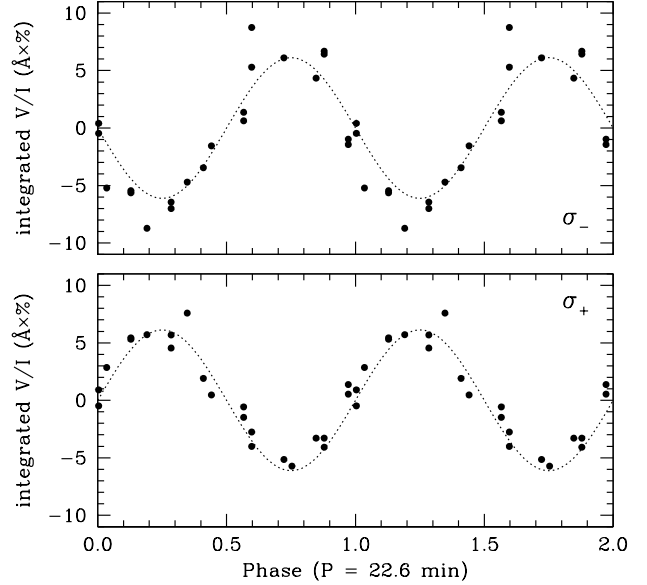


**Figure 4.** Integrated polarization measurements of the two individual  $\sigma$  components phased on the rotation period of 22.6 minutes revealing a complete reversal of the field vector. The top panel shows the measurements for the blue-shifted  $\sigma_-$  component and the bottom panel shows the measurements of the red-shifted  $\sigma_+$  component.

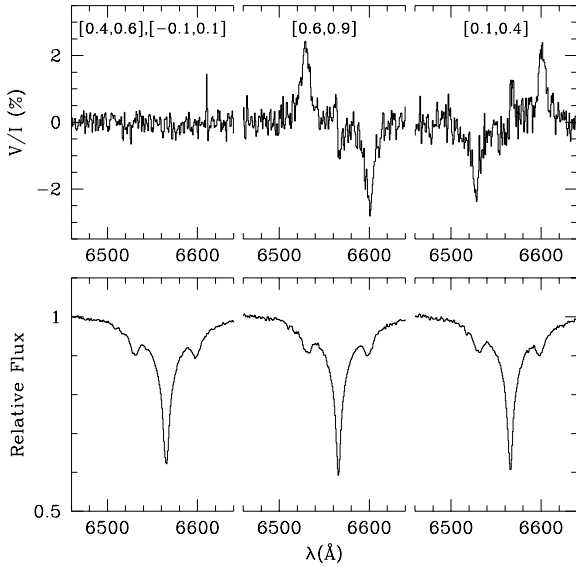
highlighting the flipping of the sigma components. The flip in the sign of the  $H\alpha$   $\sigma$  components at phases 0.1-0.4 and 0.6-0.9 and their anti-symmetric behaviour around the zero polarization spectrum of phases 0.4-0.6, indicate that the magnetic axis must be nearly perpendicular to the rotation axis of the white dwarf.

Figure 6 illustrates the geometry of the system with  $\alpha$  set at its minimum value ( $90 - i$ ). Assuming  $i = 45^\circ$  (see Section 3.3.2), the angle  $\alpha$  will vary between  $90^\circ - 45^\circ$  and  $90^\circ + 45^\circ$ . When  $\alpha \approx 90^\circ$ , the positive and negative polarization contributions cancel each other and give rise to the unpolarized, featureless spectrum observed in the phase range 0.4-0.6. This can be explained by the change, due to stellar rotation, between the magnetic field direction and the line of sight to the observer averaged over the visible hemisphere of the star (Wickramasinghe & Martin 1979). The  $\pi$  component in the circular polarisation spectra shows the presence of narrow antisymmetric circular polarisation features. These are caused by Faraday mixing due to magneto-optical effects which converts linear polarisation into circular polarisation (Martin & Wickramasinghe 1981, 1982) during the radiation transfer.

#### 3.2.1 Photometric variations

The photometric observations were analysed using three different methods described in detail by Paunzen & Vanmunster (2016). First, we employed periodic orthogonal polynomials which are particularly useful for the detection of non-sinusoidal oscillations. We fitted the observations to identify the period and employed the analysis of the variance (ANOVA) statistic to evaluate the quality of the fit (Schwarzenberg-Czerny 1996).

Next, we employed the string-length methods which simply minimize the separation between consecutive phased data points at trial periods. The best-fitting period corresponds to a minimum in



**Figure 5.** Co-added FORS2 circular polarization spectra (top panel) and flux spectra (bottom panel) at three phase ranges showing the flip in the sign of the  $\sigma$  components of  $H\alpha$ . The spectrum with zero polarization corresponds to a nearly orthogonal viewing angle to the magnetic axis.

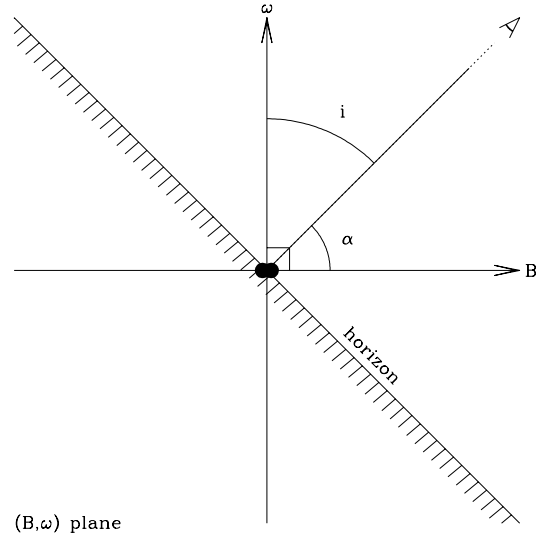


**Figure 6.** Schematic view of the geometry of the double degenerate system NLTT 12758. The rotation plane of the magnetic white dwarf is assumed to coincide with the orbital plane, and the spin axis is marked  $\omega$ . The spin axis is at an angle  $i$  with respect to the observer and the magnetic field axis  $B$  is at an angle  $\alpha$  with respect to the observer.

the “string-length” which consists of the sum of data separations. The methods are useful for sparse data sets.

Finally, The Phase Dispersion Minimization (PDM) method is similar to the string-length method (Stellingwerf 1978). In this method, the data are sorted into phase bins at trial periods and the variance within each bin is calculated. The sum of the variances is minimized at the best-fitting period.

We found that the photometric observations in the  $R$  band show variations. The calculated frequencies and their errors for the three different nights are  $65.4 \pm 1.3$ ,  $65.3 \pm 0.6$ , and  $65.6 \pm 1.2$  cycles per day, respectively. The errors depend on the individual data set lengths and the overall quality of the nights. Within the errors, these values transform to a period of  $22 \pm 0.5$  min. The semi-amplitude of the variations is 6.2 mmag. Figure 7 shows the photometric magnitudes phased on the best rotation period of 22.0 minutes with the periodogram.

We conclude that the variations in spectropolarimetry and photometry coincide and are phased on the rotation period of the magnetic white dwarf. The photometric variation may be explained in terms of magnetic dichroism which is caused by the different absorption coefficients of left and right handed circularly polarised radiation. A formulation for magnetic dichroism of hydrogen in magnetic white dwarfs was first obtained by Lamb & Sutherland (1974) and used to explain the photometric variations of the high field magnetic white dwarf EUVE J0317-855 (Ferrario et al. 1997). However the magnetic field of the DAP component of NLTT 12758 is relatively low ( $B < 20$  MG) for this effect to be important. An alternate explanation for the photometric variations could be stellar spots (Brinkworth et al. 2005). Such a spot could be formed by the inhibition of convection in the atmosphere by the magnetic field. Tremblay et al. (2015) show that convection is inhibited at the surface of objects such as the magnetic component of NLTT 12758, however their models are not able to explain flux variations like

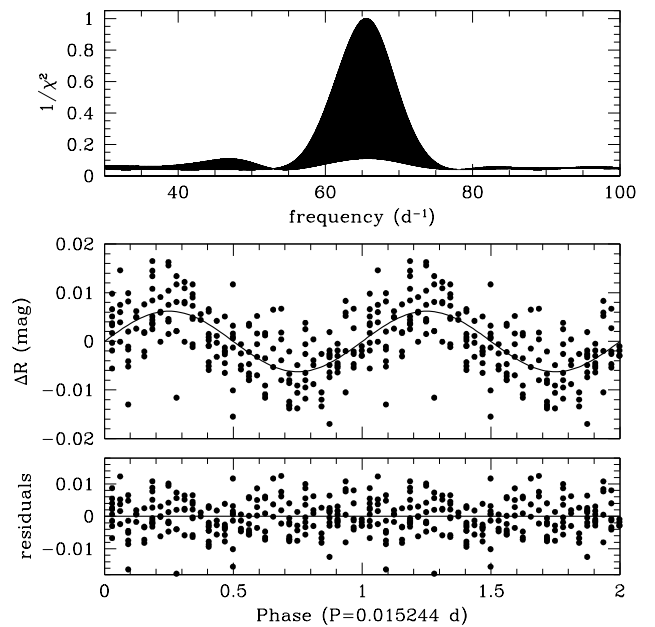


**Figure 7.** (Top panel) period analysis of the measured  $R$  photometric measurements. (Middle panel) photometric  $R$  magnitudes phased on the best rotation period and (bottom panel) residuals.

those observed in NLTT 12758 and other cool white dwarfs with low magnetic fields observed by Brinkworth et al. (2013).

### 3.3 Stellar and atmospheric parameters

#### 3.3.1 Modelling the field structure

The appearance of the spectra of magnetic white dwarfs changes dramatically as the field increases in strength. If we indicate with  $(n, l, m_l)$  the zero field quantum numbers, the linear Zeeman regime arises through the removal of the  $m_l$  degeneracy, which for the Balmer series occurs at a field strength of  $\sim 1 - 4$  MG. As the field increases, or the principal quantum number  $n$  increases, the quadratic effect becomes more important until the  $l$  degeneracy is also removed. This is called the quadratic Zeeman regime. In this regime, the wavelength shift depends on the electron excitation level and the  $\pi$  and  $\sigma$  Zeeman components are all displaced from their zero field positions by different amounts. The quadratic shift is of similar importance to the linear shift at  $B \sim 4$  MG for the higher components of the Balmer series (e.g.  $H\delta$ ). The spectra of NLTT 12758 indicate that the magnetic component of this system belongs to the low field regime, as first reported by [Kawka & Vennes \(2012a\)](#).

Before outlining our modelling methods, we need to stress that an important and as yet unsolved problem regarding the modelling of magnetic atmospheres, particularly in the high magnetic field regime, is that concerning line broadening. However in the low field regime, which is appropriate to the study of the spectrum of NLTT 12758, it is possible to assume, as a first approximation, that each Zeeman component is broadened as in the zero field case. This approach has been used successfully for the Zeeman modelling of hot white dwarfs and has allowed the determination of the mass of the hot and ultra-massive magnetic white dwarfs 1RXS J0823.6-2525 ( $B \sim 2.8 - 3.5$  MG [Ferrario et al. 1998](#)) and PG 1658+441 ( $B \sim 3.5$  MG [Ferrario et al. 1998](#); [Schmidt et al. 1992](#)). In the case of PG 1658+441, the spectroscopic mass was found to be in good agreement with that determined by the trigonometric parallax method ([Dahn 1999](#); [Vennes & Kawka 2008](#)). No trigonometric parallax is as yet available for 1RXS J0823.6-2525. On the other hand, in cool white dwarfs such as NLTT 12758, the contribution due to Stark broadening is negligible and spectral line broadening is dominated by resonance. For  $H\alpha$  to  $H\gamma$ , we used parameters from the comprehensive self-broadening theory of [Barklem et al. \(2000\)](#), and for the upper Balmer lines we combined the impact parameters from [Ali & Griem \(1965, 1966\)](#) with the van der Waals parameters as described in [Kawka & Vennes \(2012b\)](#).

The modelling of the magnetised spectrum of NLTT 12758 has been conducted as follows. First, we have computed a zero-field grid of pure hydrogen white dwarf model atmospheres (see [Kawka & Vennes 2012a](#)). We used the ML2 parameterization of the mixing length theory with  $\alpha = 0.6$ , where  $\alpha$  is the ratio of the mixing length to the pressure scale height. Convection is predicted to be suppressed in cool magnetic white dwarfs ([Tremblay et al. 2015](#)), however we will investigate the effect of suppressed convection on the spectral lines of stars such as NLTT 12758 in future work. This grid of models was then used as input for the magnetic atmosphere program of [Wickramasinghe & Martin \(1979\)](#), modified to allow for Doppler, resonance and Stark broadenings and magneto-optical effects which take into account the different refractive indices for radiation with different polarisation state ([Martin & Wickramasinghe 1981](#)). The shifts and strengths in hydrogen lines, caused by the magnetic field, are included using the results of Zeeman calculations by [Kemic \(1974\)](#). Atmospheric models were then constructed at selected points on the visible hemisphere of the white dwarf taking into consideration the changes in field strength and direction. The resulting Stokes inten-

sities were then appropriately summed to yield a synthetic spectrum.

The field geometry is strongly dependent on field strength and structure and models built on observations obtained at different phases, if the star rotates around its axis, are better constrained than those restricted to one single intensity spectrum corresponding to only one magnetic phase. The best constrained models are those based on observations at different rotational phases and for which *both* intensity and polarisation spectra are available as it is the case for NLTT 12758.

The modelling of a magnetic white dwarf usually starts with the assumption that the magnetic field configuration is that of a centred dipole. Then, if necessary, more complex structures are investigated. These usually consist of offset dipoles or combinations of higher order multipoles. For the present set of observations of NLTT 12758 we found that a centred dipole model was inadequate to model the rotationally modulated Zeeman components by simply changing the viewing angle. This is because a centred dipole allows a field spread of at most of a factor 2, which is not sufficient to model the observations of NLTT 12758. It is possible to achieve a larger magnetic field spread by offsetting the dipole from the centre of the star. If the dipole is shifted by a fraction  $a_z$  of the stellar radius along the dipole axis, then the ratio of the field strengths  $B_{p1}$  and  $B_{p2}$  at the two opposite poles become

$$\frac{B_{p1}}{B_{p2}} = \left( \frac{1 - a_z}{1 + a_z} \right)^3 \quad (1)$$

We describe in detail how we have achieved the best-fit model for NLTT 12758 in the sections that follow.

#### 3.3.2 Spectroscopic analysis

We fitted the X-shooter spectra with two sets of model spectra. The first set of model spectra are for non-magnetic hydrogen-rich white dwarfs as described in [Kawka & Vennes \(2012a\)](#). The Balmer line profiles used in the synthetic spectra calculations are described in [Kawka & Vennes \(2012b\)](#). The second set of model spectra include a magnetic field (as described above).

The procedure fits simultaneously the effective temperature and surface gravity of both white dwarfs (4 parameters). We used the mass-radius relations of [Benvenuto & Althaus \(1999\)](#) to scale the flux for both stars and ensure that the relative flux contribution of each star is preserved imposing a common distance for both stars. A similar decomposition method was adopted in the analysis of the hot double degenerate EUVE J1439+750 ([Vennes et al. 1999](#)) and in the analysis of a sample of double degenerates by [Rolland \(2014\)](#) and [Rolland & Bergeron \(2015\)](#). The results are model dependent due to uncertainties in the treatment of line broadening in the presence of a magnetic field as previously noted by [Külebi et al. \(2009\)](#). However, the presence of a non-magnetic DA companion with a reliable radius measurement, as in the case of NLTT 12758, helps constrain the radius of the magnetic component. A direct constraint on the stellar radii would be achieved with a parallax measurement.

The Zeeman splitting observed in the X-shooter spectra ( $H\alpha$  and  $H\beta$ ) implies an averaged surface field of  $B_s = 1.70 \pm 0.04$  MG. We used this value as a starting point to calculate sets of magnetic field spectra with varying polar field strength and offset. We fitted the spectra with the following magnetic field strengths and offsets: offset =  $-0.1$  at  $B_p = 2.8, 3.1, 3.4, 3.6$  MG; offset =  $0$  at  $B_p = 2.6, 3.0, 3.2, 3.4$  MG; offset =  $+0.1$  at  $B_p = 2.4, 2.9, 3.1, 3.3$  MG. We also fitted the X-shooter spectra at viewing angles of  $50^\circ$

and  $80^\circ$  for each offset and field strength value. Note that the total exposure time covers nearly two complete rotation cycles and the viewing angle represents a cycle average.

Figure 8 compares the X-shooter spectrum and the best-fitting models for the two stars. The magnetic white dwarf has a polar magnetic field  $B_p = 3.1$  MG offset by  $a_z = +0.1$  from the stellar centre. The magnetic white dwarf appears to be slightly cooler with  $T_{\text{eff,DAP}} = 7220 \pm 180$  K and a surface gravity of  $\log g = 8.16 \pm 0.08$ . The non-magnetic white dwarf is a little hotter and more massive with  $T_{\text{eff,DA}} = 7950 \pm 50$  K and  $\log g = 8.37 \pm 0.04$ . The best-fitting viewing angle to the dipole axis is on average  $\alpha = 80^\circ$ . Table 4 lists the stellar parameters. We computed the mass and cooling age of each component using the evolutionary models of [Benvenuto & Althaus \(1999\)](#). The spectroscopic mass ratio  $M_{\text{DA}}/M_{\text{DAP}} = 1.1 - 1.3$  is consistent with the orbital mass ratio, but also more accurate, and implies that the mass of the DA star may be slightly higher than the mass of the DAP star. We then estimated the absolute magnitude of each component and calculated the distance to the system.

[Rolland \(2014\)](#) and [Rolland & Bergeron \(2015\)](#) measured the stellar parameters of NLTT 12758 by fitting  $H\alpha$  together with the spectral energy distribution (SED) including only  $VJHK$ . They obtained  $T_{\text{eff,DAP}} = 6041$  K and  $T_{\text{eff,DA}} = 8851$  with a radius ratio of  $R_{\text{DA}}/R_{\text{DAP}} = 0.908$ . Although our radius ratio is in agreement with theirs, our effective temperatures differ from their effective temperatures.

Taking advantage of a broader wavelength coverage, we re-analysed the SED. First, we fitted the photometric data set ( $NUV, UVB, gri, JHK$  and  $W1, W2$ ) by fixing the surface gravity measurements to those obtained in the spectroscopic analysis. We allowed for both temperatures to vary and assumed null interstellar extinction. The resulting effective temperatures are nearly in agreement with the spectroscopic analysis showing that interstellar extinction in the line of sight toward NLTT 12758 is negligible when compared to the total extinction in the same line of sight,  $E(B - V) = 0.06$  ([Schlegel et al. 1998](#)). Figure 9 shows the model photometry fitted to the measured photometry and compares the confidence contours for the SED fit, as well as the confidence contours for the Balmer line fit (Fig. 8). The overlapping contours show that the two methods are consistent and imply that the two objects share similar stellar parameters. In the following discussion we adopt the results of the spectroscopic analysis.

Our results differ markedly from those of [Rolland \(2014\)](#) and [Rolland & Bergeron \(2015\)](#) who reported a temperature difference  $\Delta T = T_{\text{eff,DA}} - T_{\text{eff,DAP}} \approx 2800$  K while we estimated much closer temperatures for the components ( $\Delta T \approx 700$  K). On the other hand we estimated a similar mass ratio. Our spectroscopic analysis includes the first four members of the Balmer line series ( $H\alpha$  to  $H\delta$ ), thereby lifting potential degeneracy in the  $T_{\text{eff}}/\log g$  solution, while [Rolland \(2014\)](#) and [Rolland & Bergeron \(2015\)](#) only include  $H\alpha$ . However, both solutions are model dependent and part of the discrepancy may also be attributed to different line-broadening prescriptions used in calculating magnetic synthetic spectra. The large temperature difference reported by [Rolland \(2014\)](#) and [Rolland & Bergeron \(2015\)](#) should also be noticeable in the SED, particularly in the near ultraviolet. Our own analysis based on an extensive data set implies a temperature difference no larger than  $\approx 1100$  K ( $1\sigma$ ) while a larger temperature difference would be incompatible with the *GALEX* *NUV* measurement.

Using the evolutionary mass-radius relations of [Benvenuto & Althaus \(1999\)](#), we find that the cooling ages of the two white dwarfs in NLTT 12758 are comparable. However,

**Table 4.** Summary of NLTT 12758 parameters

Parameter	DA	DAP
$T_{\text{eff}}$ (K)	$7950 \pm 50$	$7220 \pm 180$
$\log g$ (c.g.s)	$8.37 \pm 0.04$	$8.16 \pm 0.08$
Mass ( $M_\odot$ )	$0.83 \pm 0.03$	$0.69 \pm 0.05$
Cooling age (Gyrs)	$2.2 \pm 0.2$	$1.9 \pm 0.4$
$M_V$ (mag)	$13.65 \pm 0.06$	$13.69 \pm 0.18$
Period (d)	$1.15401 \pm 0.00005$	
$K$ (km s $^{-1}$ )	$81.9 \pm 17.3$	$89.7 \pm 3.8$
$\gamma$ (km s $^{-1}$ )	$94.2 \pm 17.3$	$96.4 \pm 2.6$
$d$ (pc)	$32.6 \pm 3.5$	
$v_r$ (km s $^{-1}$ )	$58.0 \pm 3.9$	

[Valyavin et al. \(2014\)](#) have proposed that convection in cool white dwarfs is suppressed by magnetic fields, and therefore magnetic white dwarfs may appear younger than they are. The 3D radiation magnetohydrodynamic simulations of [Tremblay et al. \(2015\)](#) have confirmed that magnetic fields do suppress convection, however they do not affect the cooling of the white dwarf until temperatures have dropped below 6000 K. Since the magnetic white dwarf is hotter than this upper limit, it is likely that its age is not affected and that the two objects formed around the same time.

We derived an orbital inclination of  $i = 45^\circ$  for NLTT 12758 by combining the component masses with the orbital parameters and using:

$$\frac{M_{\text{DA}}^3 \sin^3 i}{(M_{\text{DA}} + M_{\text{DAP}})^2} = \frac{PK_{\text{DAP}}^3}{2\pi G} \quad (2)$$

where  $M_{\text{DA}}$  and  $M_{\text{DAP}}$  are the masses of the non-magnetic and magnetic white dwarfs respectively,  $P$  is the orbital period,  $K_{\text{DAP}}$  is the velocity semi-amplitude of the magnetic white dwarf and  $G$  is the gravitational constant. Setting the system inclination at  $i = 90^\circ$ , the maximum orbital period is  $P \approx 3.3$  d.

The calculated white dwarf gravitational redshifts ( $\gamma_{g,\text{DAP}} = 38.4 \pm 2.9$ ,  $\gamma_{g,\text{DA}} = 53.6 \pm 1.7$  km s $^{-1}$ ) may be subtracted from their respective systemic velocities to obtain an estimate of the radial velocity of the system. Using the more precise velocity of the DAP star we obtain  $v_r = 58.0 \pm 3.9$  km s $^{-1}$ . Combining the proper motion measurements ([Kawka & Vennes 2012a](#)), the photometric distance estimate ( $d$ ) and the radial velocity ( $v_r$ ) of the system we determine the Galactic velocity components ( $U, V, W$ ) =  $(-40 \pm 4, -48 \pm 5, -3 \pm 6)$  km s $^{-1}$  which suggest that the system is relatively young and belongs to the thin disc ([Pauli et al. 2006](#)).

### 3.4 Evolution of NLTT 12758

In order to understand the evolution of NLTT 12758 we have used the rapid binary star evolution algorithm, *bse*, of [Hurley, Tout & Pols \(2002\)](#). We have evolved a number of binaries from the Zero Age Main Sequence (ZAMS) to the age of the Galactic disc (9.5 Gyr, e.g. [Oswalt et al. 1996](#); [Liu & Chaboyer 2000](#)). This code is a derivation of the single star evolution code of [Hurley, Pols & Tout \(2000\)](#) where the authors use analytical formulae to approximate the full evolution of stars. The *bse* takes into consideration stellar mass-loss, mass transfer, Roche lobe overflow, CE evolution, tidal interaction, supernova kicks and angular momentum loss caused by gravitational radiation and magnetic braking. In order to model the CE evolution, the *bse* uses the  $\alpha_{\text{CE}}$  formalism, where  $\alpha_{\text{CE}}$  is a parameter with values in the range 0.1–0.9. In our calculations we have adopted  $\eta = 1.0$  for the Reimers’



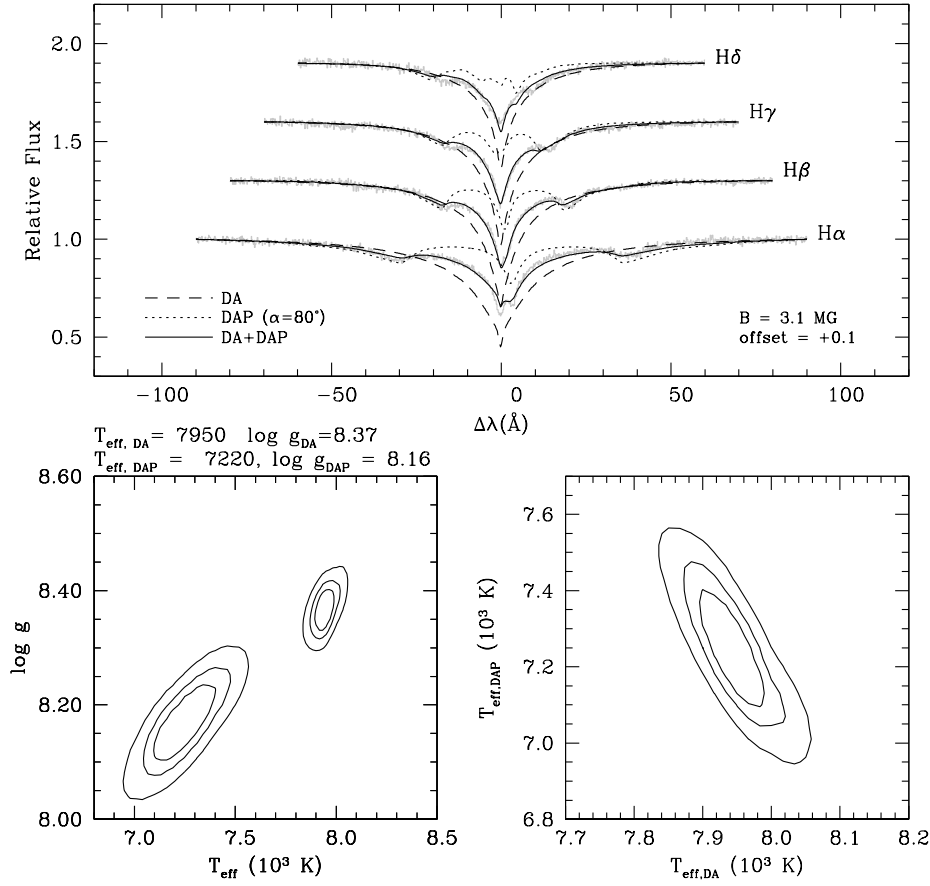


**Figure 8.** (Top panel) observed Balmer line profiles of NLTT 12758 compared to the best-fitting models. The best-fit shows that the components of NLTT 12758 are a non-magnetic DA white dwarf (dashed lines) paired with a magnetic DA white dwarf (dotted lines). Confidence contours at 66, 90, and 99% are shown in the  $T_{\text{eff,DAP}}$  vs  $T_{\text{eff,DA}}$  plane (bottom right) and  $\log g$  vs  $T_{\text{eff}}$  for both stars (bottom left).

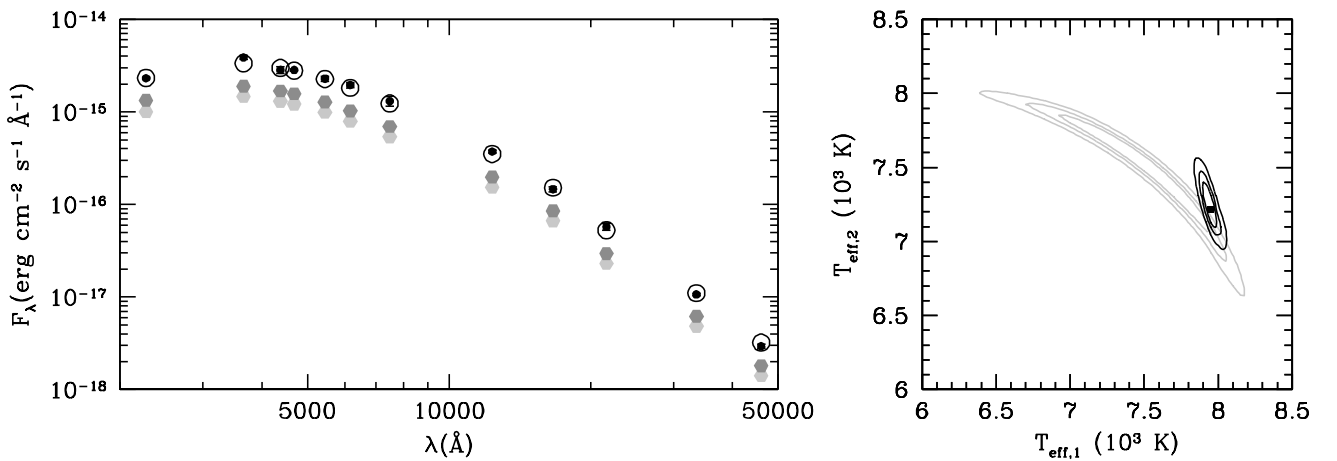


**Figure 9.** The left panel compares the best-fitting photometry (open circle) to the observed photometry (solid black circles). The contribution of individual stars are plotted in different grey shades as hexagonals. The right panel plots the confidence contours (66, 90, and 99%) of the spectroscopic fit (in black) and the contours of the SED fit (grey full lines). Note that  $\log g = 8.4$  for star 1 (DA) and  $\log g = 8.2$  for star 2 (DAP).

mass-loss parameter, as outlined in Briggs et al. (2015) and a stellar metallicity,  $Z = 0.02$ .

We have then generated a synthetic population of binaries with ZAMS conditions of the mass of the primary star,  $M_1$ , between 3.5 and 4.5  $M_\odot$ , the mass of the secondary star,  $M_2$ , between 2.5 and 3.5  $M_\odot$  and the initial period  $P_0$  in the range 2000 – 3500 days, as these values were in the region of the expected initial conditions for the final properties of the components of NLTT 12758. We allowed 200 steps in each parameter in the BSE evolution of the population through to the age of the Galactic disk. In all cases we assumed an initially circular orbit for the progenitor binary, that is, an eccentricity of zero. The calculations were repeated for values of  $\alpha_{\text{CE}} = \{0.10, 0.20, 0.25, 0.30, 0.40, 0.50, 0.60, 0.70, 0.80, 0.90\}$ .

A number of stellar types are recognised by BSE within its logic throughout the stages of evolution. These types are set out in Table 1 of Briggs et al. (2015).

The evolved populations were searched for systems that resulted in a pair of Carbon/Oxygen white dwarfs (CO WDs), that is, type 11s in the BSE system. We have found that as  $\alpha_{\text{CE}}$  increases the number of CO WD double degenerate systems increases. However, not all of these systems correspond with the type of evolution path that would lead to the final parameters of NLTT 12758, i.e. cooling ages, period, masses.

A suitable near match to NLTT 12758 was achieved at  $\alpha_{\text{CE}} = 0.15$  with initial masses of 3.75  $M_\odot$  and 2.80  $M_\odot$  and with an initial period of 2656 days. As BSE consists of many approximations, the resulting solution is considered to be satisfactory and within the errors on the parameters of NLTT 12758 given in Table 4.

The evolution shown in Table 5 starts with two stars, S1 and S2, and follows each of them through their normal evolution until 256 Myr. Up until this time the only interactions between the two stars are small mass losses due to winds and the consequent small changes in orbital separation and period. At 256 Myr the stars start to interact by common envelope evolution. First, the more massive star, S1, develops an extended envelope which overflows the Roche lobe. This draws the stars closer together by friction eroding the orbit. When Roche lobe overflow ceases and S1 reveals its core as a CO WD, the two stars are about 588  $R_\odot$  apart with a period of around 864 days. At this point, S2 is still a main sequence star. About 315 Myr later, S2 initiates its own common envelope evolution resulting in a second CO WD, an orbital separation of 5.3  $R_\odot$  and a period of only 1.161 days. One of the pair, S2, is now a magnetic WD resulting from the dynamo effect within the common envelope. S1 loses about 2.8  $M_\odot$  during the first common envelope phase while S2 loses about 2  $M_\odot$ . As the second common envelope evolution brings the two stars very close together by shrinking the orbit from about 500 to 5  $R_\odot$ , it is S2 that develops the magnetic field and the rapid rotation.

From this time the pair interact by gravitational radiation and magnetic braking with consequent orbital shrinkage until at 2791 Myr they reach the present day with a separation of 5.278  $R_\odot$  and an orbital period of 1.154 days. The cooling ages are 2535 Myr and 2220 Myr for the non-magnetic and magnetic white dwarfs respectively (for details of the method see Briggs et al. 2015). Further evolution will see the orbit shrinking further until at some stage (over a time much longer than a Hubble time) Roche lobe overflow restarts and the two stars merge. The possible final fate of double degenerate white dwarf systems, such as NLTT 12758, is discussed in the section below.

## 4 DISCUSSION

NLTT 12758 is a member of a growing class of double degenerate systems consisting of two white dwarfs, one magnetic and one not. Table 6 lists the currently known double degenerate systems containing at least one magnetic white dwarf. The table lists the names, orbital and rotational periods, the magnetic field strength, effective temperatures and masses of the components. It includes both close binaries and CPM systems. Most of the systems for which effective temperatures and masses are determined appear to have formed, within uncertainties, at the same time. In the case of CPM systems, where it is assumed that the stars did not interact during their evolution, there are systems with inconsistencies in their ages if one assumes single star evolution for each star. Apart from the well documented case of EUVE J0317-855 (Ferrario et al. 1997), another more recent example is given by PG 1258+593 and its common proper motion magnetic white dwarf companion SDSS J1300+5904. Girven et al. (2010) found that the masses of these white dwarfs are  $0.54 \pm 0.06 M_\odot$  for the non-magnetic and  $0.54 \pm 0.01 M_\odot$  for the magnetic component. Despite their very similar masses, SDSS J1300+5904 is a cool white dwarf ( $T_{\text{eff}} = 6300 \pm 300$  K) while PG 1258+593 is substantially hotter ( $T_{\text{eff}} = 14790 \pm 77$  K). Girven et al. (2010) find that the temperature discrepancy gives a difference in cooling age (and thus in formation age of the white dwarfs) of  $1.67 \pm 0.05$  Gyr. If one makes the plausible assumption that the progenitors of these CPM white dwarfs formed in the same protostellar cloud at roughly the same time, then the similar white dwarf masses and their large age discrepancy give rise to a paradox. A possible solution is that this system was initially a triple system where two stars interacted and merged to form the magnetic white dwarf SDSS J1300+5904 about 1.67 Gyr before the third non-interacting object evolved into the non-magnetic white dwarf PG 1258+593.

However, the situation appears to be rather different for the double degenerate system NLTT 12758, as reported in section 3.4. Since NLTT 12758 is a close binary system, it is highly unlikely that the field of the magnetic component was caused by the merging of two stars in an initially triple system. Instead, the magnetic field must have originated during CE evolution in a manner very similar to that occurring during the formation of a magnetic cataclysmic variable, as proposed by Briggs et al. (2016) (in preparation). In this scenario, the closer the cores of the two stars are drawn during CE evolution, the greater the differential rotation and thus the larger the dynamo generated field will be. If CE evolution leads to the merging of the two stellar cores the resulting object would be an isolated highly magnetic white dwarf (see Wickramasinghe et al. 2014). If the two stars do not coalesce they are expected to emerge from the CE as close binaries that are already interacting, and thus appear as magnetic cataclysmic variables, or are close to interaction. The low-accretion rate polars, where a magnetic white dwarf accretes matter from its companion through a stellar wind, have been suggested by Schwöpe et al. (2009) to be the progenitors of the polars, which are the highest field magnetic cataclysmic variables. In the polars a magnetic white dwarf accretes matter from an un-evolved low-mass (M-dwarf) companion via magnetically confined accretion flows. The orbital periods are typically between 70 minutes to a few hours and Zeeman and cyclotron spectroscopy from the UV to the IR bands have revealed the presence of fields between 7 to 230 MG (e.g. see Ferrario et al. 1992, 1993, 1996; Schmidt et al. 2001) in the case of the polars, and 1 to 20 MG in the case of intermediate polars (Ferrario, Wickramasinghe & King 1993). The difference between these systems and NLTT 12758 is

**Table 5.** Evolution of a binary star system of approximately the size of NLTT 12758 starting from ZAMS through to the end of their interaction and the production of a double degenerate WD pair.  $M1$  and  $M2$  are the masses of the primary and secondary stars respectively (in solar masses),  $S1$  and  $S2$  are the stellar types varying throughout their evolution as shown in Table 1 in Briggs et al. (2015).  $Sepr$  is the stellar separation in solar radii,  $Period$  is the orbital period in days and the *Event – Type* is the event happening to the system at the time given in column 2.

Step	Time (MYr)	M1 ( $M_{\odot}$ )	M2 ( $M_{\odot}$ )	S1	S2	Period (days)	Sepr ( $R_{\odot}$ )	Event-Type
1	0.000	3.750	2.800	1	1	2656.000	1510.578	ZAMS
2	210.988	3.750	2.800	2	1	2653.321	1509.562	S1⇒Hertzsprung Gap
3	212.057	3.750	2.800	3	1	2653.713	1509.674	S1⇒RGB
4	212.955	3.747	2.800	4	1	2655.573	1510.204	S1⇒He core burning
5	253.754	3.676	2.800	5	1	2714.292	1526.805	S1⇒Early AGB
6	255.551	3.597	2.801	6	1	2668.247	1503.396	S1⇒Late AGB
7	255.989	2.787	2.827	6	1	2819.839	1493.233	Begin Roche lobe overflow
8	255.989	0.827	2.827	11	1	864.356	588.342	CEE, S1⇒CO WD
9	255.989	0.827	2.827	11	1	864.356	588.342	End Roche lobe overflow
10	443.089	0.827	2.827	11	1	864.356	588.342	S2⇒Blue straggler
11	449.391	0.827	2.827	11	2	864.356	588.342	S2⇒Hertzsprung Gap
12	452.151	0.827	2.826	11	3	864.520	588.398	S2⇒RGB
13	455.303	0.827	2.824	11	4	865.691	588.810	S2⇒He core burning
14	567.390	0.827	2.774	11	5	889.679	596.911	S2⇒Early AGB
15	570.808	0.828	2.725	11	6	757.173	533.592	S2⇒Late AGB
16	571.109	0.828	2.662	11	6	689.277	498.253	Begin Roche lobe overflow
17	571.109	0.828	0.652	11	11	1.161	5.297	CEE, S2⇒CO WD
18	571.109	0.828	0.652	11	11	1.161	5.297	End Roche lobe overflow
19	2791.209	0.828	0.652	11	11	1.154	5.278	Present Day

that both progenitor stars of NLTT 12758 were too massive to evolve into a magnetic cataclysmic variable. However, the indications seem to be that the magnetic white dwarf component of NLTT 12758 acquired its field via a mechanism similar to that propounded to explain the origin of magnetic cataclysmic variables.

The properties of NLTT 12758 mean that the two white dwarfs will coalesce in a time much longer than a Hubble time ( $\sim 140$  Gyr; Ritter 1986), however it is still interesting to speculate what the final fate of a system like this might be.

The first simulations of two merging CO WDs were conducted by Saio & Nomoto (1985) and showed that the fast mass accretion rate ( $\gtrsim 10^{-5} M_{\odot} \text{yr}^{-1}$ ) from the less massive to the more massive white dwarf ignites an off-centre carbon flash. The carbon nuclear burning then propagates toward the stellar centre turning the CO WD into an ONe WD quiescently. The outcome of such an event would not be a carbon deflagration but an accretion induced collapse (AIC) triggered by electron captures on  $^{24}\text{Mg}$  and  $^{20}\text{Ne}$ . The result would be a rapidly spinning neutron star that would appear as an isolated millisecond pulsar (MSP, e.g. Lorimer 2008). The low space velocities of isolated MSPs suggest that there could not have been a substantial SNII kick imparted to the emerging neutron star, thus supporting the AIC hypothesis (Ferrario & Wickramasinghe 2007; Hurley et al. 2010). The calculations of Chen et al. (2013) lend further support to this idea since they show that it is unlikely that the isolated MSPs may be generated via the LMXB recycling scenario because this would require the total ablation of their donor star. Thus, merging events of systems similar to NLTT 12758, but with initial parameters that would allow faster evolutionary timescales, could provide a simple explanation for the existence of isolated MSPs.

On the other hand, the merging of the two stars in NLTT 12758 may give rise to a supernova event. Recent simulations conducted by Dan et al. (2014) and Dan et al. (2015) showed that a merging system with a total mass  $M_{\text{tot}} \geq 2.1 M_{\odot}$  and comprised of two white

dwarfs of similar mass may result in a Type Ia supernova; The total mass of NLTT 12758,  $M_{\text{tot}} = 1.52 M_{\odot}$ , would be below the predicted cutoff for this event to occur. However, other studies conducted by Pakmor et al. (2011) and Sato et al. (2016) found that systems with a mass ratio greater than  $\sim 0.8$  could indeed result into a SNIa explosion. Clearly, a consensus in this area of research still needs to be reached (e.g. Ferrario 2013).

## 5 CONCLUSIONS

In this paper we have reported our studies on the close, super-Chandrasekhar double degenerate system NLTT 12758 consisting of two CO WDs of similar masses and ages and with one of the two components highly magnetic. The magnetic white dwarf spins around its axis with a period of 23 minutes and they orbit around each other with a period of 1.15 days. Although the components of NLTT 12758 will not merge over a Hubble time, systems with very similar initial parameters will come into contact and merge thus undergoing either an accretion induced collapse to become a rapidly spinning neutron star (an isolated MSP) or a Type Ia supernova explosion. Given the theoretical uncertainties, the jury is still out on the fate of such systems.

## ACKNOWLEDGEMENTS

AK and SV acknowledge support from the Grant Agency of the Czech Republic (P209/12/0217 and 15-15943S) and the Ministry of Education of the Czech Republic (LG14013). This work was also supported by the project RVO:67985815 in the Czech Republic. SV acknowledges support from the Mathematical Sciences Institute of the Australian National University. EP acknowledges support by the Ministry of Education of the Czech Republic

**Table 6.** Known double degenerates containing a magnetic white dwarf

Name	Alternate name	$P_{\text{orb}}$	$P_{\text{rot}}$	$B$ (MG)	$T_{\text{eff}}$ (K)		Mass ( $M_{\odot}$ )		Reference
					Magnetic	Companion	Magnetic	Companion	
0040+000	SDSS J004248.19+001955.3	...	...	14	11000		...	...	1
0121-429 <sup>a</sup>	LHS 1243	...	...	10.3	6105	5833	0.7 <sup>d</sup>	0.54 <sup>d</sup>	2,3,4
0239+109 <sup>a</sup>	G 4-34, LTT 10886	...	...	0.7	10060	7620	...	...	5,6
0325-857	EUVE J0317-855	~ 2095 yr	725 s	185-425	33000	16360	1.3	0.85	7,8,9,10
0410-114	NLTT 12758, G160-51	1.15 d	23 min	3.1	7220	7950	0.69	0.83	This work
0512+284 <sup>a</sup>	LSPM J0515+2839	...	...	2.15	5940	6167	0.81 <sup>d</sup>	0.61 <sup>d</sup>	3,4
0745+303	SDSS J074853.07+302543.5	CPM	...	11.4	21000	22702	0.81	0.88	11
0843+488 <sup>b</sup>	SDSS J084716.21+484220.4	...	...	...	19000		...	...	1
0924+135	SDSS J092646.88+132134.5	CPM	...	210	9500	10482	0.62	0.79	12
0945+246	LB 11146	~ 130 d	...	~ 670	16000	14500	0.90	0.91	13,14,15
1026+117 <sup>a</sup>	LHS 2273	...	...	17.8	5691	7350	0.75 <sup>d</sup>	0.64 <sup>d</sup>	3,4
1258+593	SDSS J130033.48+590407.0	CPM	...	6	6300	14790	0.54	0.54	16
1330+015 <sup>a</sup>	G 62-46	...	...	7.4	5712	7618	0.82 <sup>d</sup>	0.64 <sup>d</sup>	3,4
1440+753	EUVE J1439+750	...	...	10	42000	30000	0.9	1.1	17
1503-070 <sup>a</sup>	GD 175	...	...	2.9	6062	7051	0.95 <sup>d</sup>	0.73 <sup>d</sup>	3,4
1506+399	CBS 229	CPM	...	18.9	18000	16761	0.81	0.82	11
1506+523	SDSS J150746.80+520958.0	CPM	...	65.2	18000	17622	0.99	0.70	12
1514+282 <sup>a</sup>	SDSS J151625.07+280320.9	...	...	2.05	7168	7662	0.77 <sup>d</sup>	0.54 <sup>d</sup>	3,4
1713+393 <sup>a</sup>	NLTT 44447	...	...	2.1	6204	6556	0.94 <sup>d</sup>	0.54 <sup>d</sup>	3,4,18
1814+248 <sup>c</sup>	G 183-35	...	...	12.05/7.8	5998	5849	0.85 <sup>d</sup>	0.74 <sup>d</sup>	3,4,19
1818+126 <sup>a</sup>	G 141-2	...	...	3.75	5215	6451	0.64 <sup>d</sup>	0.54 <sup>d</sup>	3,4

<sup>a</sup> DAH+DC<sup>b</sup> DAH+DB<sup>c</sup> DAH+DAH<sup>d</sup> Masses are calculated using the mass-radius relations of [Benvenuto & Althaus \(1999\)](#), the published parameters of the magnetic star and ratio of the stellar radii.References: (1) [Schmidt et al. \(2003\)](#); (2) [Subasavage et al. \(2007\)](#); (3) [Rolland \(2014\)](#); (4) [Rolland & Bergeron \(2015\)](#); (5) [Koester et al. \(2009\)](#); (6) [Gianninas et al. \(2011\)](#); (7) [Ferrario et al. \(1997\)](#); (8) [Vennes et al. \(2003\)](#); (9) [Külebi et al. \(2010\)](#); (10) [Lawrie \(2013\)](#); (11) [Dobbie et al. \(2013\)](#); (12) [Dobbie et al. \(2012\)](#); (13) [Nelan \(2007\)](#); (14) [Glenn et al. \(1994\)](#); (15) [Liebert et al. \(1993\)](#); (16) [Girven et al. \(2010\)](#); (17) [Vennes et al. \(1999\)](#); (18) [Kawka & Vennes \(2006\)](#); (19) [Putney \(1995\)](#)

(grant LG15010). GPB gratefully acknowledges receipt of an Australian Postgraduate Award. We thank the referee, Pier-Emmanuel Tremblay, for a thorough report and helpful comments on line-broadening theory.

## REFERENCES

Alecian E. et al., 2015, in IAU Symp. 307, Meynet G., Georgy C., Groh J., Stee P., eds., Vol. 307, Geneva, Switzerland, pp. 330  
 Ali A. W., Griem H. R., 1965, Phys. Rev. A, 140, 1044  
 Ali A. W., Griem H. R., 1965, Phys. Rev. A, 144, 366  
 Barstow M. A., Jordan S., O'Donoghue D., Burleigh M. R., Napiwotzki R., Harrop-Allin M. K., 1995, MNRAS, 277, 971  
 Angel J. R. P., Borra E. F., Landstreet J. D., 1981, ApJS, 45, 457  
 Aznar Cuadrado R., Jordan S., Napiwotzki R., Schmid H. M., Solanki S. K., Mathys G., 2004, A&A, 423, 1081  
 Barklem P. S., Piskunov N., O'Mara B. J., 2000, A&A, 363, 1091  
 Benvenuto O. G., Althaus L. G., 1999, MNRAS, 303, 30  
 Briggs G. P., Ferrario L., Tout C. A., Wickramasinghe D. T., Hurley J. R., 2015, MNRAS, 447, 1713  
 Briggs G. P., Ferrario L., Tout C. A., Wickramasinghe D. T., 2016, MNRAS, to be submitted  
 Brinkworth C. S., Burleigh M. R., Lawrie K., Marsh T. R., Knigge C., 2013, ApJ, 773, 47  
 Brinkworth C. S., Marsh T. R., Morales-Rueda L., Maxted P. F. L., Burleigh M. R., Good S. A., 2005, MNRAS, 357, 333  
 Cardelli J. A., Clayton G. C., Mathis J. S., 1989, ApJ, 345, 245  
 Chen H-L, Chen X., Tauris T. M., Han Z., 2013, ApJ, 775, 27  
 Cutri R. M., et al., 2012, VizieR Online Data Catalog, 2311

Dahn C. C., 1999, 11th European Workshop on White Dwarfs, ASP Conference Series, 169, 24  
 Dan M., Guillochon J., Brüggen M., Ramirez-Ruiz E., Rosswog S., 2015, MNRAS, 454, 4411  
 Dan M., Rosswog S., Brüggen M., Podsiadlowski P., 2014, MNRAS, 438, 14  
 Dobbie P. D., Baxter R., Külebi B., Parker Q. A., Koester D., Jordan S., Lodieu N., Euchner F., 2012, MNRAS, 421, 202  
 Dobbie, P.D. et al., 2013, MNRAS, 428, L16  
 Eggen O. J., 1968, ApJ, 153, 195  
 Ferrario L., Wickramasinghe D. T., Bailey J. A., Hough J. H., Tuohy I. R., 1992, MNRAS, 256, 252  
 Ferrario L., Bailey J., Wickramasinghe D. T., 1993, MNRAS, 262, 285  
 Ferrario L., Bailey J., Wickramasinghe D. T., 1996, MNRAS, 282, 218  
 Ferrario L., 2012, MNRAS, 426, 2500  
 Ferrario L., Vennes S., Wickramasinghe D. T., 1998, MNRAS, 299, L1.  
 Ferrario L., Vennes S., Wickramasinghe D. T., Bailey J. A., Christian D. J., 1997, MNRAS, 292, 205  
 Ferrario L., 2013, "Binary Paths to Type Ia Supernovae Explosions", Proc. IAU Symposium No 281, Cambridge University Press, Cambridge (UK), Eds: R. Di Stefano, M. Orio, M. Moe, Vol. 281, p. 341  
 Ferrario L., de Martino D., Gänsicke, B. T., 2015a, Space Science Review, 191, 111  
 Ferrario L., Melatos A., Zrake J., 2015b, Space Science Review, 191, 77  
 Ferrario L., & Wickramasinghe D. T., 2007, MNRAS, 375, 1009  
 Ferrario L., Wickramasinghe D. T., King A. R. 1993, MNRAS, 260, 149  
 Fouqué P. et al., 2000, A&A, 141, 313  
 García-Berro E. et al., 2012, ApJ, 749, 25  
 Gianninas A., Bergeron P., Ruiz M. T., 2011, ApJ, 743, 138  
 Girven J., Gänsicke B. T., Külebi B., Steeghs D., Jordan S., Marsh T. R.,



- Koester D., 2010, MNRAS, 404, 159
- Glenn J., Liebert J., Schmidt G. D., 1994, PASP, 106, 722
- Henden A. A., Templeton M., Terrell D., et al. 2016, VizieR Online Data Catalog, 2336
- Hollands M. A., Gänsicke B. T., Koester D., 2015, MNRAS, 450, 681
- Hurley J. R., Pols O. R., Tout C. A., 2000, MNRAS, 315, 543
- Hurley J. R., Tout C. A., Pols O. R., 2002, MNRAS, 329, 897
- Hurley, J. R., Tout, C. A., Wickramasinghe, D. T., Ferrario, L., Kiel, P. D. 2010, MNRAS, 402, 1437
- Kawka A., Vennes S. 2004, in IAU Symp. 224, The A-Star Puzzle, ed. J. Zverko, et al. (Cambridge U. Press), 879
- Kawka A., Vennes S., 2006, ApJ, 643, 402
- Kawka A., Vennes S., 2012a, MNRAS, 425, 1394
- Kawka A., Vennes S., 2012b, A&A, 538, A13
- Kawka A., Vennes S., 2014, MNRAS, 439, L90
- Kawka A., Vennes S., Schmidt G. D., Wickramasinghe D. T., Koch R. 2007, ApJ, 654, 499
- Kemic S. B., 1974, JILA REP. No. 113
- Kepler S. O. et al., 2013, MNRAS, 429, 2934
- Koester D., Voss B., Napiwotzki R., Christlieb N., Homeier D., Lisker T., Reimers D., Heber U., 2009, A&A, 505, 441
- Külebi B., Jordan S., Euchner F., Gänsicke B. T., Hirsch H. 2009, A&A, 506, 1341
- Külebi B., Jordan S., Nelan E., Bastian U., Altmann M., 2010, A&A, 524, A36
- Lamb F. K., Sutherland P. G., 1974, IAUS, 53, 265
- Landstreet J. D., Bagnulo S., Valyavin G. G., Fossati L., Jordan S., Monin D., Wade G. A., 2012, A&A, 545, A30
- Lawrie K. A., 2013, PhD Thesis, University of Leicester
- Liebert J., Bergeron P., Holberg J. B., 2003, AJ, 125, 348
- Liebert J., Bergeron P., Schmidt G. D., Saffer R. A., 1993, ApJ, 418, 426
- Liebert J., Ferrario L., Wickramasinghe D. T., Smith P. S. 2015, ApJ, 804, 93
- Liebert J. et al. 2005, AJ, 129, 2376
- Liu W. M., Chaboyer B., 2000, ApJ, 544, 818
- Lorimer D. R. 2008, Living Rev. Relativity 11, 8
- Martin B., Wickramasinghe D. T. 1981, MNRAS, 196, 23
- Martin B., Wickramasinghe D. T. 1982, MNRAS, 200, 993
- Maxted P. F. L., Ferrario L., Marsh T. R., Wickramasinghe D. T., 2000, MNRAS, 315, L41
- Morrissey P., et al., 2007, ApJS, 173, 682
- Nelan E. P., 2007, AJ, 134, 1934
- Nordhaus J., Wellons S., Spiegel D. S., Metzger B. D., Blackman E. G., 2011, PNAS, 108, 3135
- Oswalt T. D., Smith J. A., Wood M. A., Hintzen P., 1996, Nature, 382, 692
- Pakmor R., Hachinger S., Röpke F. K., Hillebrandt W., 2011, A&A, 528, A117
- Pauli E.-M., Napiwotzki R., Heber U., Altmann M., Odenkirchen M., 2006, A&A, 447, 173
- Paunzen E., Vanmunster T., 2016, AN, 337, 239
- Potter A. T., Tout C. A., 2010, MNRAS, 402, 1072
- Putney A., 1995, ApJL, 451, L67
- Ritter H., 1986, A&A, 169, 139
- Rolland B. 2014, M.Sc. Thesis, Université de Montréal
- Rolland B., Bergeron P., 2015, ASP Conference Ser., 493, 53
- Saio H. & Nomoto K., 1985, A&A, 150, L21
- Sato Y., Nakasato N., Tanikawa A., Nomoto K., Maeda K., Hachisu I., 2016, ApJ, 821, 67
- Schlegel D. J., Finkbeiner D. P., Davis M. 1998, ApJ, 500, 525
- Schmidt G. D., Bergeron P., Liebert J., Saffer R., 1992, ApJ, 394, 603
- Schmidt G. D., Smith P. S., 1995, ApJ, 448, 305
- Schmidt G. D., Vennes S., Wickramasinghe D. T., Ferrario L., 2001, MNRAS, 328, 203
- Schmidt G. D., Ferrario L., Wickramasinghe D. T., Smith P. S., 2001, ApJ, 553, 823
- Schmidt G. D., et al., 2003, ApJ, 595, 1101
- Schwarzenberg-Czerny A., 1996, ApJ, 460, L107
- Schwöpe A.D., Nebot Gomez-Moran A., Schreiber M.R., Gänsicke B.T. 2009, A&A, 500, 867
- Skrutskie M. F., 2006, AJ, 131, 1163
- Stellingwerf, R. F. 1978, ApJ, 224, 953
- Stetson, P. B. 1987, PASP, 99, 191
- Subasavage J. P., Henry T. J., Bergeron P., Dufour P., Hambly N. C., Beaulieu T. D., 2007, AJ, 134, 252
- Tout C. A., Wickramasinghe D. T., Ferrario L., 2004, MNRAS, 355, L13
- Tout C. A., Wickramasinghe D. T., Liebert J., Ferrario L., Pringle J. E., 2008, MNRAS, 387, 897
- Tremblay P.-E., Fontaine G., Freytag B., Steiner O., Ludwig H.-G., Steffen, M., Wedemeyer S., Brassard P. 2015, ApJ, 812, 19
- Valyavin G., Wade G. A., Bagnulo S., Szeifert T., Landstreet J. D., Han I., Burenkov A., 2008, ApJ, 683, 466
- Valyavin G., et al. 2014, Nature, 515, 88
- Vennes S., Ferrario L., Wickramasinghe D. T., 1999, MNRAS, 302, L49
- Vennes S., Kawka A., 2008, MNRAS, 389, 1367
- Vennes S., Schmidt G. D., Ferrario L., Christian D. J., Wickramasinghe D. T., Kawka A., 2003, ApJ, 593, 1040
- Vernet J., et al., 2011, A&A, 536, 105
- Wade G. A., et al., 2016, MNRAS, 456, 2
- Wickramasinghe D. T., Ferrario L., 2000, PASP, 112, 873
- Wickramasinghe D. T., Ferrario L., 2005, MNRAS, 356, 1576
- Wickramasinghe D. T., Martin B. 1979, MNRAS, 188, 165
- Wickramasinghe D. T., Tout C. A., Ferrario L. 2014, MNRAS, 437, 675
- York D. G., et al. 2000, AJ, 120, 1579